

RESEARCH ARTICLE

Dynamic Characteristic Improvement of Battery Charger for PMDs Using a Model Predictive Control

GWANYOUNG MOON¹, (Student Member, IEEE), AND YEONGSU BAK², (Member, IEEE)¹Department of Electronic and Electrical Engineering, Keimyung University, Daegu 42601, South Korea²Department of Electrical Energy Engineering, Keimyung University, Daegu 42601, South Korea

Corresponding author: Yeongsu Bak (ysbak@kmu.ac.kr)

This work was supported by the National Research Foundation of Korea (NRF) Grant funded by the Korea Government [Ministry of Science and ICT (MSIT)] under Grant RS-2022-00165694.

ABSTRACT This paper proposes a dynamic characteristics improvement of battery charger for personal mobility devices (PMDs) using a model predictive control (MPC). The battery charger is used to charge a battery of PMDs such as electric scooters, electric bicycles, and electric skateboards and an output voltage of the battery charger is generally controlled by a proportional-integral (PI) controller. The PI controller requires a gain tuning to improve a dynamic characteristic, however, an overshoot of the output voltage can be occurred in transient state when the gain is increased. Therefore, to improve the dynamic characteristic of the battery charger for PMDs, this paper presents the MPC method to control the output voltage of the battery charger for PMDs. The effectiveness of the proposed MPC method is proved by the simulation and experimental results.

INDEX TERMS Battery charger, personal mobility devices (PMDs), model predictive control (MPC) method, dynamic characteristic.


I. INTRODUCTION

Recently, an abnormal climate phenomena have occurred due to environmental pollution and global warming caused by carbon dioxide [1], [2], [3]. It causes human and material damage and raise awareness of carbon dioxide emissions worldwide. Therefore, interest in electric-mobility (E-mobility), an eco-friendly which means of transportation that can replace internal combustion engine vehicles, is increasing to reduce carbon dioxide emissions [4], [5], [6]. Additionally, the use of e-mobility has significant potential to contribute to the 'double carbon' goals of the traditional transport sector by reducing carbon dioxide emissions [7].

Various types of energy storage devices are used in e-mobility [8]. In general, the E-mobility is driven by using electricity from a built-in battery as power, and it is classified depending on travel distance. E-mobility for long-distance

travel includes electric vehicles, plug-in hybrid vehicles, and hydrogen electric vehicles. On the other hand, E-mobility for short-distance travel includes electric scooters, electric bicycle, electric skateboards [9], [10], [11], which are also called a personal mobility devices (PMDs). The PMDs are accessible because it can be used in various space such as bicycle roads and pedestrian roads, additionally, they are portable because the size of them is convenient to carry. Due to these advantages, the demand for PMDs is rapidly increasing, and the related market is gradually expanding [12], [13].

The battery voltage of PMDs has a wide range depending on the type of PMDs such as electric scooters, electric bicycles, and electric skateboards. In general, individual battery chargers according to the type of PMDs are used to charge the battery of PMDs with a single rated voltage [14], [15], [16]. The individual battery chargers reduce industrial usability and availability of PMDs. Therefore, in recent, the battery charger which is able to charge the battery of PMDs with

The associate editor coordinating the review of this manuscript and approving it for publication was Guillermo Valencia-Palomo .

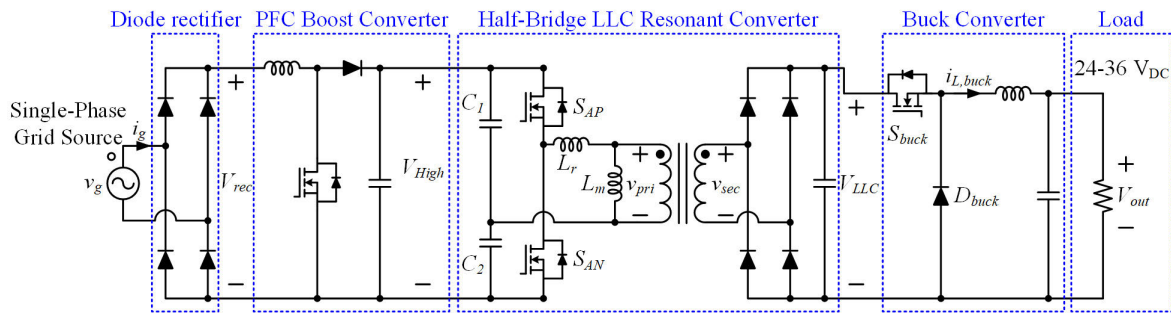


FIGURE 1. Circuit configuration of the battery charger for PMDs.

various voltages from 24 V to 72 V has been developed in order to improve industrial usability and availability of PMDs [17], [18], [19].

The battery charger with wide range of output voltage is generally constructed using several power conversion devices. In [17], the battery charger is constructed by a multi-level DC-DC converter which is connecting several buck converters in series. However, since universal AC voltage cannot be used as an input voltage of the battery charger, the industrial usability of PMDs is reduced. In [18], it is constructed by a boost converter and a half-bridge (HB) LLC resonant converter. However, it is difficult to generate a wide range of output voltage using a frequency control of the HB LLC resonant converter. In [19], the battery charger is constructed by a three-stage structure using a boost converter, a HB LLC resonant converter, and a buck converter. It has advantages that universal AC voltage is able to the input voltage of the battery charger and it is easy to generate a wide range of output voltage using the buck converter.

In general, an output voltage of the battery charger is controlled by a proportional-integral (PI) controller to charge a battery of PMDs because it has advantages of simple structure and easy implementation. In the PI controller, the proportional control is related to the dynamic characteristics of the control element in transient state and the integral control is related to the error of the control element in steady state [20], [21], [22]. In other words, the performance of the PI controller is determined by the gain of the proportional and integral control and an appropriate gain tuning is required to improve dynamic characteristics. However, the gain tuning for improving dynamic characteristics has limitations due to the possibility that the overshoot of control elements occurs in transient state [23], [24], [25], [26]. Additionally, although the above-mentioned rule-based strategies have high execution efficiency, they cannot achieve optimal control because they rely on expert experience when setting the bandwidth considering the interactions between control loops [27]. To overcome these disadvantages of the PI controller, a model predictive control (MPC) method can be used. Contrary to PI controller, MPC method has relatively excellent control performance because it does not need to set the bandwidth without considering the interaction between control loops. In the past, the MPC method was difficult to apply to the system

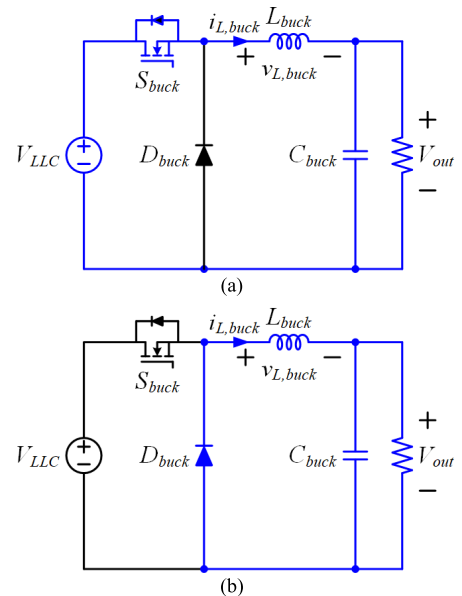


FIGURE 2. Equivalent operating circuit of the buck converter in a steady state. (a) Mode 1. (b) Mode 2.

due to its high computational process. However, in recent years, with the development of efficient control algorithms and computer hardware, the MPC method has become applicable to the systems [27], [28], [29].

Therefore, in this paper, a dynamic characteristic improvement of battery charger for PMDs using the MPC method is proposed. In the proposed MPC method, a cost function is designed by the modeling of the battery charger for PMDs and the optimal control input of the battery charger is decided to the duty of the buck converter by minimizing the cost function. Therefore, it can obtain fast dynamic characteristic of the battery charger without gain tuning contrary to the PI controller. The effectiveness of the proposed MPC method for the battery charger for PMDs is proved by the simulation and experimental results.

II. CIRCUIT CONFIGURATION AND OPERATION PRINCIPLE OF BATTERY CHARGER

A. CIRCUIT CONFIGURATION

Fig. 1 shows the circuit configuration of the battery charger for PMDs with a wide range of output voltage. The battery

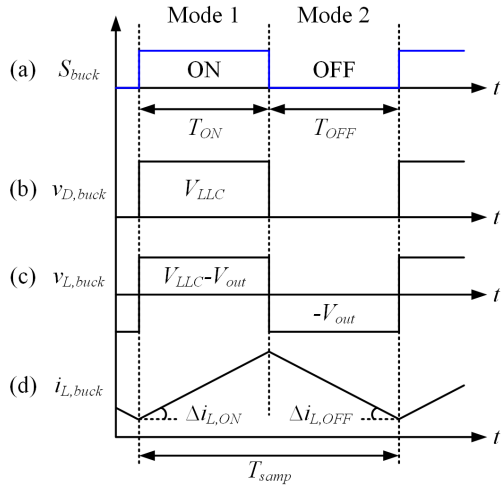


FIGURE 3. Voltage and current waveforms depending on the switching state of the buck converter. (a) Switching state. (b) Diode voltage. (c) Inductor voltage. (d) Inductor current.

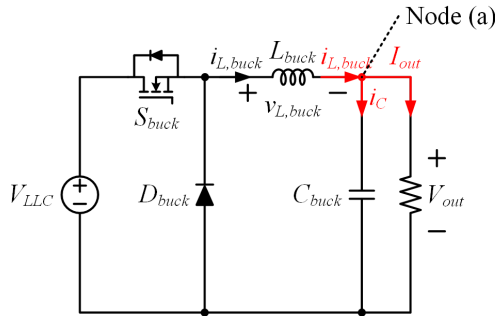


FIGURE 4. Circuit configuration to obtain the variation of output voltage.

charger for PMDs consists of three main parts: a power factor correction (PFC) boost converter, a HB LLC resonant converter, and a buck converter. In addition, a single-phase grid source and a diode rectifier are connected to the input stage of the PFC boost converter and a load is connected to the output stage of the buck converter.

Firstly, the PFC boost converter controls an output voltage (V_{High}) to 400 V from the voltage (V_{rec}) rectified by the diode rectifier. It also performs PFC by equaling the phase between voltage (v_g) and the current (i_g) of the single-phase grid source. For this purpose, UCC28180 which is the control IC from TI was used to perform current and voltage controller. Secondly, the HB LLC resonant converter has two power semiconductor switches (S_{AP} and S_{AN}), a transformer that electrically separates the single-phase grid source from the battery, and a diode rectifier. The primary side voltage (v_{pri}) of the transformer is generated by the S_{AP} and S_{AN} operating in complementary switching state with duty ratios of 0.5 and the secondary side voltage (v_{sec}) of the transformer is reduced by turn-ratio. It performed open loop control with a fixed switching frequency. Additionally, an output voltage (V_{LLC}) of the HB LLC resonant converter is generated by the diode rectifier. Lastly, the buck converter consists of a power

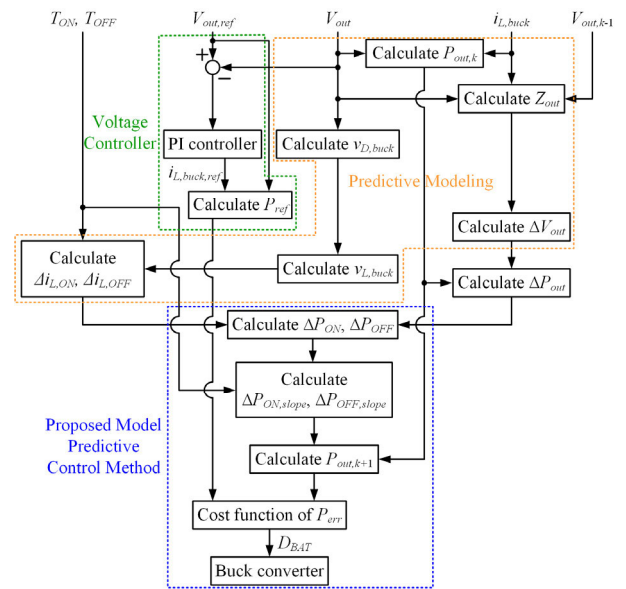


FIGURE 5. Control block diagram of the proposed MPC method for the battery charger.

semiconductor switch (S_{buck}) and a schottky diode (D_{buck}) and the load connected to the buck converter uses a resistor instead of the battery. The buck converter controls the output voltage (V_{out}) of the battery charger with wide range.

B. OPERATION PRINCIPLE OF BUCK CONVERTER

Fig. 2 shows the equivalent operating circuit of the buck converter in a steady state. It is divided into two modes, Mode 1 and Mode 2, depending on the switching state of S_{buck} . In Mode 1 as shown in Fig. 2(a), S_{buck} is ON state and V_{LLC} is applied to D_{buck} . The voltage ($v_{L,buck}$) applied to the inductor is a difference between V_{LLC} and V_{out} and it increases the inductor current ($i_{L,buck}$). In addition, in Mode 2 as shown in Fig. 2(b), S_{buck} is OFF state and V_{LLC} is blocked by S_{buck} . $v_{L,buck}$ is $-V_{out}$ and it decreases the $i_{L,buck}$.

Fig. 3 shows the voltage and current waveforms depending on the switching state of the buck converter. In Fig. 3(a), the switching state of S_{buck} is changed to OFF state from ON state during a control period (T_{samp}). Additionally, the switching time of S_{buck} during ON and OFF state is expressed as in (1).

$$\begin{aligned} T_{ON} &= D_{BAT} T_{samp}, \\ T_{OFF} &= (1 - D_{BAT}) T_{samp}, \end{aligned} \quad (1)$$

where D_{BAT} is the duty ratio of S_{buck} .

As shown in Fig. 3(b), the voltage applied into the D_{buck} is V_{LLC} and 0 during T_{ON} and T_{OFF} , respectively. In addition, as shown in Fig. 3(c), the voltage applied into the L_{buck} is $V_{LLC} - V_{out}$ and $-V_{out}$ during T_{ON} and T_{OFF} , respectively. As a result, they are expressed as in (2) and (3) depending on the Mode 1 and Mode 2.

$$v_{D,buck} = \begin{cases} V_{LLC} & (\text{when Mode 1}), \\ 0 & (\text{when Mode 2}). \end{cases} \quad (2)$$

TABLE 1. Simulation parameters.

Parameters	Values
Single-phase grid source	220 V _{rms} /60 Hz
Transformer turn-ratio	17:8
Output capacitor	980 μF
Output inductor	87 μH
Resistor of load	3 Ω
Control Period	1.5 μs

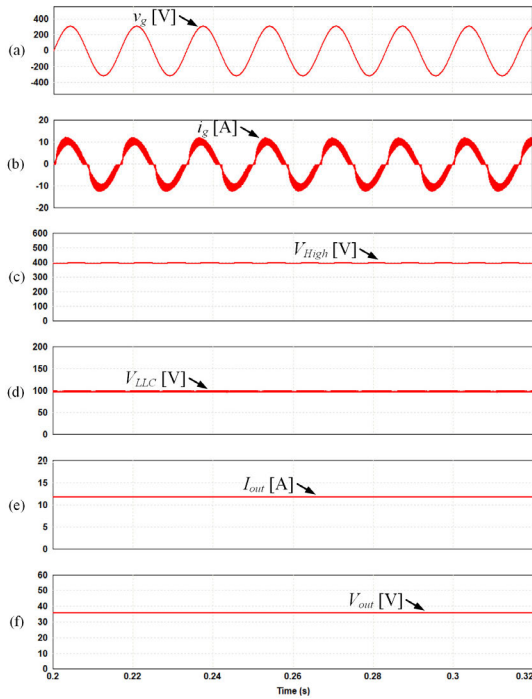


FIGURE 6. Simulation results of operation principles of the battery charger for PMDs. (a) Voltage of single-phase grid source. (b) Current of single-phase grid source. (c) Output voltage of the PFC boost converter. (d) Output voltage of the HB LLC resonant converter. (e) Output current of the battery charger. (f) Output voltage of the battery charger.

$$v_{L,buck} = \begin{cases} V_{LLC} - V_{out} & (\text{when Mode 1}), \\ -V_{out} & (\text{when Mode 2}). \end{cases} \quad (3)$$

In Fig. 3(d), $i_{L,buck}$ is changed by the magnitude of the $v_{L,buck}$. The $i_{L,buck}$ is increased in Mode 1 with positive magnitude of the $v_{L,buck}$ during T_{ON} , on the other hand, $i_{L,buck}$ is decreased in Mode 2 with negative magnitude of the $v_{L,buck}$ during T_{OFF} .

The inductor voltage of the buck converter is expressed as in (4).

$$\begin{aligned} v_{L,buck} &= L_{buck} \frac{di_{L,buck}}{dt}, \\ di_{L,buck} &= \frac{v_{L,buck}}{L_{buck}} dt. \end{aligned} \quad (4)$$

The variation of $i_{L,buck}$ is expressed as in (5).

$$\Delta i_{L,buck} = \frac{T_{samp}}{L_{buck}} v_{L,buck}. \quad (5)$$

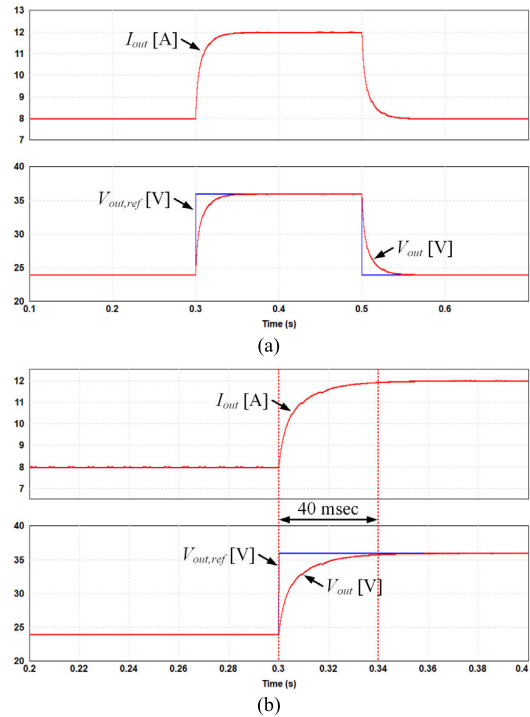


FIGURE 7. Simulation results of the output voltage control of the battery charger using the PI controller. (a) Reference voltage is changed between 24 V and 36 V. (b) Expanded waveform.

From (1), (3), and (5), the variation of $i_{L,buck}$ depending on T_{ON} and T_{OFF} are expressed as in (6).

$$\begin{aligned} \Delta i_{L,ON} &= \left(\frac{T_{ON}}{L_{buck}} \right) (V_{LLC} - V_{out}) \\ &= \left(\frac{D_{BAT} T_{samp}}{L_{buck}} \right) (V_{LLC} - V_{out}), \\ \Delta i_{L,OFF} &= \left(\frac{T_{OFF}}{L_{buck}} \right) (0 - V_{out}) \\ &= \left(\frac{(1 - D_{BAT}) T_{samp}}{L_{buck}} \right) (0 - V_{out}). \end{aligned} \quad (6)$$

III. PROPOSED MPC METHOD FOR BATTERY CHARGER

A. PREDICTIVE MODELING OF BUCK CONVERTER

Fig. 4 shows the circuit configuration to obtain the variation of V_{out} . In Fig. 4, applying Kirchhoff's current law to the node (a), $i_{L,buck}$ is expressed as in (7).

$$i_{L,buck} = i_C + I_{out} = C_{buck} \frac{dV_{out}}{dt} + I_{out}, \quad (7)$$

where i_C is the current flowing into the capacitor (C_{buck}) of the buck converter and I_{out} is the current flowing into the load.

From (7), the variation of V_{out} is calculated as in (8).

$$\begin{aligned} \frac{dV_{out}}{dt} &= \frac{\Delta V_{out}}{T_{samp}} = \frac{1}{C_{buck}} (i_{L,buck} - I_{out}), \\ \Delta V_{out} &= \frac{T_{samp}}{C_{buck}} (i_{L,buck} - I_{out}) = \frac{T_{samp}}{C_{buck}} \left(i_{L,buck} - \frac{V_{out}}{Z_{out}} \right), \end{aligned} \quad (8)$$

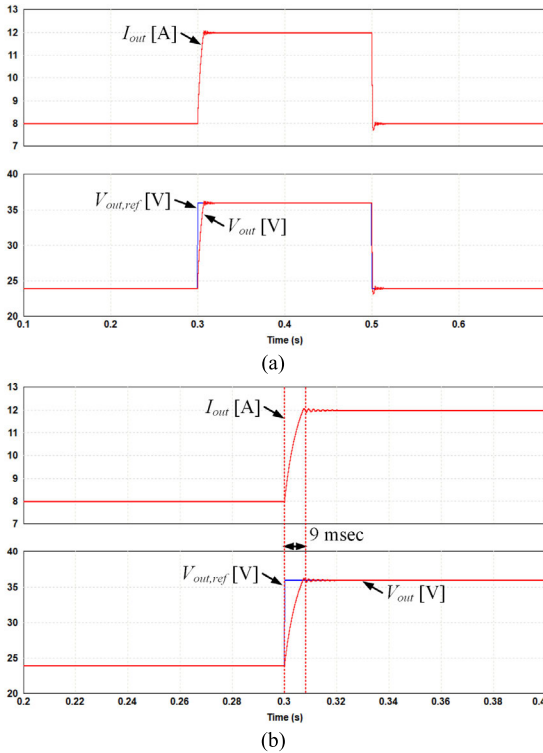


FIGURE 8. Simulation results of the output voltage control of the battery charger using the proposed MPC method. (a) Reference voltage is changed between 24 V and 36 V. (b) Expanded waveform.

where Z_{out} is the impedance of the load. Additionally, ΔV_{out} can be rewritten as in (9).

$$\Delta V_{out} \cong V_{out,k} - V_{out,k-1} = \frac{T_{samp}}{C_{buck}} \left(i_{L,buck} - \frac{V_{out}}{Z_{out}} \right), \quad (9)$$

where $V_{out,k}$ and $V_{out,k-1}$ are the voltages in a present and a previous control period, respectively. Therefore, from (9), Z_{out} can be estimated as in (10).

$$Z_{out} = \frac{V_{out}}{i_{L,buck} - \left(\frac{C_{buck}}{T_{samp}} \right) (V_{out,k} - V_{out,k-1})}. \quad (10)$$

In addition, the output power of the battery charger in the present control period is expressed as in (11).

$$P_{out,k} = V_{out,k} i_{L,buck}, \quad (11)$$

Using the variation of the V_{out} and $i_{L,buck}$, the output power in the next control period is calculated as in (12).

$$\begin{aligned} P_{out,k+1} &= (V_{out,k} + \Delta V_{out}) (i_{L,buck} + \Delta i_{L,buck}) \\ &= V_{out,k} i_{L,buck} + V_{out,k} \Delta i_{L,buck} \\ &\quad + \Delta V_{out,k} i_{L,buck} + \Delta V_{out,k} \Delta i_{L,buck} \end{aligned} \quad (12)$$

B. PROPOSED MPC METHOD

Fig. 5 shows the control block diagram of the proposed MPC method for the battery charger. It is classified into a PI-based voltage controller, a predictive modeling, and the

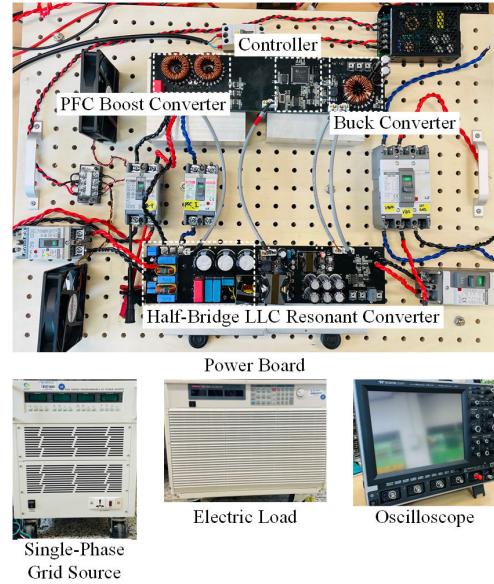


FIGURE 9. Experimental setup of the battery charger for PMDs.

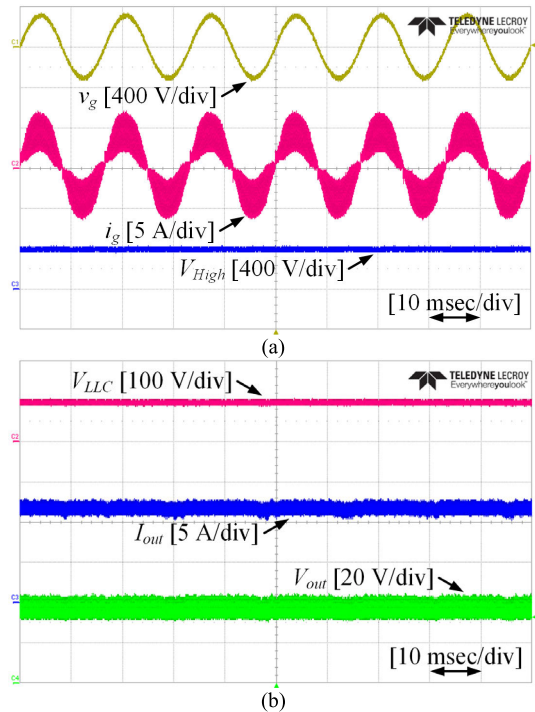


FIGURE 10. Experimental results of operation principles of the battery charger for PMDs.

proposed MPC method. In the PI-based voltage controller, V_{out} is controlled to the reference output voltage ($V_{out,ref}$) and the reference inductor current ($i_{L,buck,ref}$) can be calculated. In the predictive modeling, Z_{out} and ΔV_{out} are calculated as in (10) and (8). In addition, $\Delta i_{L,ON}$ and $\Delta i_{L,OFF}$ are calculated as in (6). Finally, in the proposed MPC method, $P_{out,k+1}$ as in (12) can be rewritten as in (13).

$$P_{out,k+1} = P_{out,k} + \Delta P_{out}, \quad (13)$$

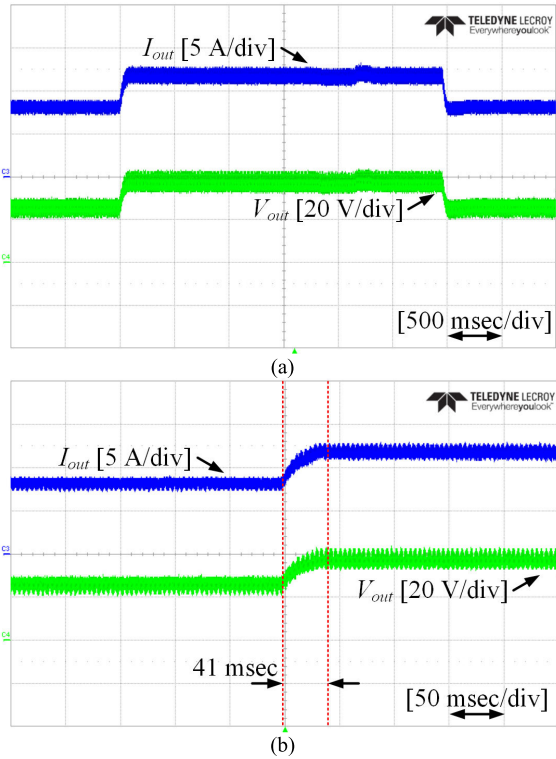


FIGURE 11. Experimental results of the output voltage control of the battery charger using the PI controller. (a) Reference voltage is changed between 24 V and 36 V. (b) Expanded waveform.

where ΔP_{out} is the variation of the output power of the battery charger. Applying (12) into (13), ΔP_{out} is calculated as in (14).

$$\begin{aligned} \Delta P_{out} &= P_{out,k+1} - P_{out,k} \\ &= V_{out,k} i_{L,buck} + V_{out,k} \Delta i_{L,buck} \\ &\quad + \Delta V_{out,k} i_{L,buck} + \Delta V_{out,k} \Delta i_{L,buck} - V_{out,k} i_{L,buck} \\ &= V_{out} \Delta i_{L,buck} + \Delta V_{out} i_{L,buck} + \Delta V_{out} \Delta i_{L,buck}. \end{aligned} \quad (14)$$

From (14), the variation of the output power depending on T_{ON} and T_{OFF} is expressed as in (15) by using $\Delta i_{L,ON}$ and $\Delta i_{L,OFF}$ as in (6).

$$\begin{aligned} \Delta P_{ON} &= V_{out} \Delta i_{L,ON} + \Delta V_{out} i_{L,buck} + \Delta V_{out} \Delta i_{L,ON}, \\ \Delta P_{OFF} &= V_{out} \Delta i_{L,OFF} + \Delta V_{out} i_{L,buck} + \Delta V_{out} \Delta i_{L,OFF}. \end{aligned} \quad (15)$$

Additionally, the slope of the ΔP_{ON} and ΔP_{OFF} is calculated as in (16).

$$\begin{aligned} \Delta P_{ON,slope} &= \frac{V_{out} \Delta i_{L,ON} + \Delta V_{out} i_{L,buck} + \Delta V_{out} \Delta i_{L,ON}}{T_{ON}}, \\ \Delta P_{OFF,slope} &= \frac{V_{out} \Delta i_{L,OFF} + \Delta V_{out} i_{L,buck} + \Delta V_{out} \Delta i_{L,OFF}}{T_{OFF}}. \end{aligned} \quad (16)$$

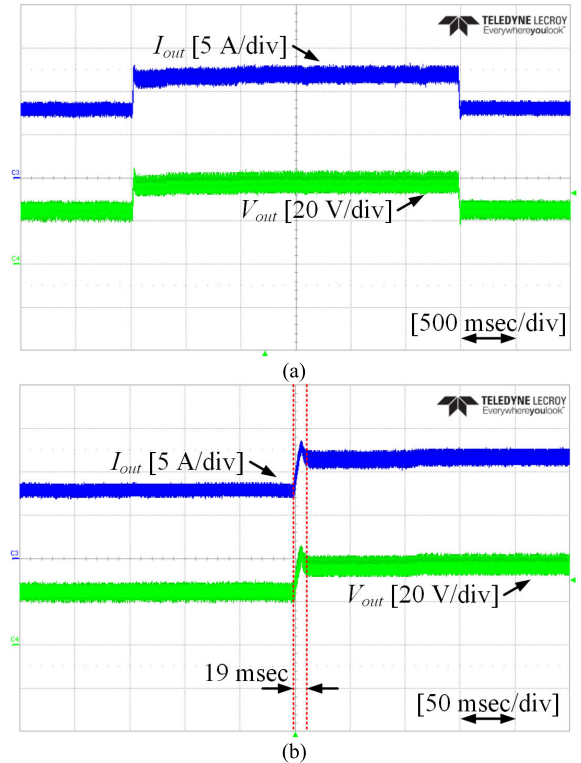


FIGURE 12. Experimental results of the output voltage control of the battery charger using the proposed MPC method. (a) Reference voltage is changed between 24 V and 36 V. (b) Expanded waveform.

Considering the ΔP_{out} depending on T_{ON} and T_{OFF} during a control period, $P_{out,k+1}$ can be calculated as in (17).

$$P_{out,k+1} = P_{out,k} + \Delta P_{ON,slope} T_{ON} + \Delta P_{OFF,slope} T_{OFF}. \quad (17)$$

Applying (1) into (17), $P_{out,k+1}$ is calculated as in (18).

$$\begin{aligned} P_{out,k+1} &= P_{out,k} + \Delta P_{ON,slope} D_{BAT} T_{samp} \\ &\quad + \Delta P_{OFF,slope} (1 - D_{BAT}) T_{samp}. \end{aligned} \quad (18)$$

In the proposed MPC method, the cost function is defined as in (19) with the error of the output power. The cost function consists of parameters derived by performing predictive modeling based on system design parameters according to system requirements. The system requirements include T_{samp} as in (1), L_{buck} as in (6), and C_{buck} as in (9).

$$\begin{aligned} P_{err} &= P_{ref} - P_{out,k+1} \\ &= P_{ref} - P_{out,k} - \Delta P_{ON,slope} D_{BAT} T_{samp} \\ &\quad - \Delta P_{OFF,slope} (1 - D_{BAT}) T_{samp}, \end{aligned} \quad (19)$$

where P_{ref} is the reference output power, which is expressed as in (20).

$$P_{ref} = V_{out,ref} i_{L,buck,ref}, \quad (20)$$

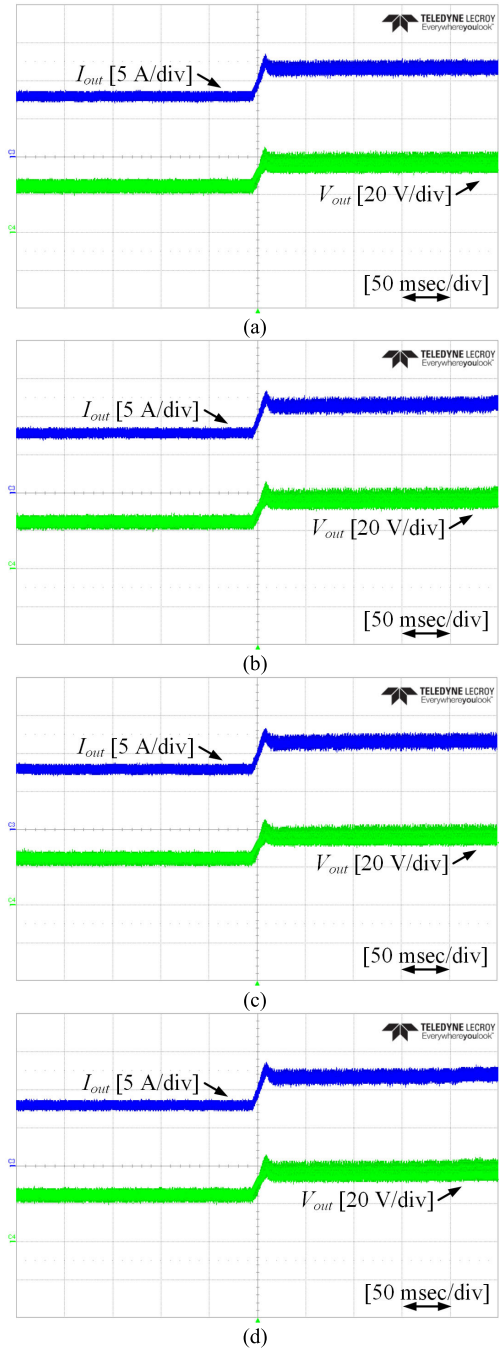


FIGURE 13. Experimental results of the output voltage control of the battery charger when the modeling parameters were mismatched. (a) $0.5 L_{buck}/C_{buck}$. (b) $1.5 L_{buck}/C_{buck}$. (c) $L_{buck}/0.5 C_{buck}$. (d) $L_{buck}/1.5 C_{buck}$.

Finally, in (19), P_{err} as the cost function is set to zero and it can be rewritten as in (21). By setting the cost function to zero, the duty ratio is derived according to the slope of the ΔP_{ON} and ΔP_{OFF} . The duty ratio is input to the power semiconductor switch of the buck converter and it controls the V_{out} to the $V_{out,ref}$ according to the duty ratio.

$$P_{ref} - P_{out,k} = \Delta P_{ON,slope} D_{BAT} T_{samp} + \Delta P_{OFF,slope} (1 - D_{BAT}) T_{samp}. \quad (21)$$

As a result, through the proposed MPC method, D_{BAT} as the duty ratio of S_{buck} can be calculated as in (22).

$$D_{BAT} = \frac{P_{ref} - P_{out,k} - \Delta P_{OFF,slope} D_{BAT} T_{samp}}{(\Delta P_{ON,slope} - \Delta P_{OFF,slope}) T_{samp}}. \quad (22)$$

IV. SIMULATION RESULTS

In this paper, simulations were performed to prove the effectiveness of the proposed MPC method for the battery charger. The simulation parameters are listed in Table 1. The switching frequency is set to 80 kHz and the control period is set to 12.5 μ s.

Fig. 6 shows the simulation results of operation principles of the battery charger for PMDs. Figs. 6(a) and (b) show the v_g and i_g and the phase of them are equal through the PFC boost converter. Additionally, as shown in Fig. 6(c), V_{High} is controlled to 400 V by the PFC boost converter. Fig. 6(d) shows the V_{LLC} , which is a 100 V. Finally, as shown in Figs. 6(e) and (f), I_{out} and V_{out} are controlled to 12 A and 36 V, respectively.

Fig. 7 shows the simulation results of the output voltage control of the battery charger using the PI control. In Fig. 7, $V_{out,ref}$ is changed to 36 V from 24 V at 0.3 s, additionally, it is changed to 24 V from 36 V at 0.5 s. V_{out} is controlled to $V_{out,ref}$ by using the PI controller. In these simulation results, the bandwidth of the PI-based current and voltage controller is set to 3000 Hz and 150 Hz, respectively, considering the switching frequency. Therefore, the proportional and integral gain of the current controller were 0.369 and 783, additionally, they of the voltage controller were 0.132 and 9.4. As shown in Fig. 7(b), which is expanded waveform, the settling time of V_{out} to reach 36 V is approximately 40 ms in the transient state.

Fig. 8 shows the simulation results of the output voltage control of the battery charger using the proposed MPC method. It has the same scenario as that shown in Fig. 7 and V_{out} is controlled to $V_{out,ref}$ by using the proposed MPC method. As shown in Fig. 8(b), which is expanded waveform, the settling time of V_{out} to reach 36 V is approximately 9 ms in the transient state. Compared to Fig. 7(b), it was confirmed that the dynamic characteristic of the battery charger is improved about four times.

V. EXPERIMENTAL RESULTS

In this paper, to prove the effectiveness of the proposed MPC method for the battery charger, the experiments were conducted using the experimental setup as shown in Fig. 9. The experimental setup consists of the power board, single-phase grid source, the electric load, and oscilloscope. The experimental parameters are completely identical with the simulation parameters listed in Table 1. In the power board, the controller is constructed using a digital signal processor (DSP), which is TMS320F28335 and the proposed MPC method is programmed into the DSP.

Fig. 10 shows the experimental results of operation principles of the battery charger for PMDs. In Fig. 10(a), the

phase of v_g and i_g are equal and V_{High} is controlled to 400 V through the PFC boost converter. In Fig. 10(b), V_{LLC} is a 100 V, additionally, I_{out} and V_{out} are controlled to 12 A and 36 V, respectively.

Fig. 11 shows the experimental results of the output voltage control of the battery charger using the PI control. It has the same scenario as that shown in Fig. 7 and V_{out} is controlled to 24 V and 36 V, respectively, by using the PI controller. As shown in Fig. 11(b), which is expanded waveform, the settling time of V_{out} to reach 36 V is approximately 41 ms in the transient state.

Fig. 12 shows the experimental results of the output voltage control of the battery charger using the proposed MPC method. It has the same scenario as that shown in Fig. 11 and V_{out} is controlled to 24 V and 36 V, respectively, by using the proposed MPC method. As shown in Fig. 12(b), which is expanded waveform, the settling time of V_{out} to reach 36 V is approximately 19 ms in the transient state. Compared to Fig. 11(b), it was confirmed that the dynamic characteristic of the battery charger is improved more than two times.

Fig. 13 shows the experimental results of the output voltage control of the battery charger when the modeling parameters were mismatched. It has the same scenario as that shown in Fig. 12 except the modeling parameters mismatch. In Fig. 13(a), the experimental result is performed by changing L_{buck} , which is the inductance of the inductor that consist of the buck converter, to 0.5 times. In Fig. 13(b), the experimental result is performed by changing L_{buck} to 1.5 times. In Fig. 13(c), the experimental result is performed by changing C_{buck} , which is the capacitance of the capacitor that consist of the buck converter, to 0.5 times. In Fig. 13(d), experimental result is performed by changing C_{buck} to 1.5 times. Although the L_{buck} and the C_{buck} were changed, the output voltage was controlled by using the proposed MPC method. As a result, it was proved that the proposed MPC method is robust in the case of the modeling parameters mismatch.

VI. CONCLUSION

This paper proposed the dynamic characteristic improvement of the battery charger for PMDs using the MPC method. Battery charger for PMDs is used to charge the battery of PMDs such as electric scooters, electric bicycle, and electric skateboards and the output voltage of the battery charger is generally controlled by the PI controller. However, the PI controller requires a gain tuning to improve a dynamic characteristic. Therefore, to improve the dynamic characteristic of the battery charger for PMDs, this paper presents the MPC method to control the output voltage of the battery charger for PMDs. In addition, the proposed MPC method is robust in the case of the modeling parameters mismatch. The effectiveness of the proposed MPC method is verified by the simulation and experimental results.

REFERENCES

- [1] A. Haddoun, M. E. H. Benbouzid, D. Diallo, R. Abdessemed, J. Ghouili, and K. Srairi, "Modeling, analysis, and neural network control of an EV electrical differential," *IEEE Trans. Ind. Electron.*, vol. 55, no. 6, pp. 2286–2294, Jun. 2008, doi: 10.1109/TIE.2008.918392.
- [2] M. Vasiladiotis and A. Rufer, "A modular multiport power electronic transformer with integrated split battery energy storage for versatile ultra-fast EV charging stations," *IEEE Trans. Ind. Electron.*, vol. 62, no. 5, pp. 3213–3222, May 2015, doi: 10.1109/TIE.2014.2367237.
- [3] G. Waltrich, M. A. M. Hendrix, and J. L. Duarte, "Three-phase bidirectional DC/DC converter with six inverter legs in parallel for EV applications," *IEEE Trans. Ind. Electron.*, vol. 63, no. 3, pp. 1372–1384, Mar. 2016, doi: 10.1109/TIE.2015.2494001.
- [4] K.-Y. Lo, Y.-M. Chen, and Y.-R. Chang, "MPPT battery charger for stand-alone wind power system," *IEEE Trans. Power Electron.*, vol. 26, no. 6, pp. 1631–1638, Jun. 2011, doi: 10.1109/TPEL.2010.2088405.
- [5] D.-G. Woo, D.-M. Joo, and B.-K. Lee, "On the feasibility of integrated battery charger utilizing traction motor and inverter in plug-in hybrid electric vehicles," *IEEE Trans. Power Electron.*, vol. 30, no. 12, pp. 7270–7281, Dec. 2015, doi: 10.1109/TPEL.2015.2396200.
- [6] D. Moon, J. Park, and S. Choi, "New interleaved current-fed resonant converter with significantly reduced high current side output filter for EV and HEV applications," *IEEE Trans. Power Electron.*, vol. 30, no. 8, pp. 4264–4271, Aug. 2015, doi: 10.1109/TPEL.2014.2360470.
- [7] X. Zhang, Z. Lu, X. Yuan, Y. Wang, and X. Shen, "L2-gain adaptive robust control for hybrid energy storage system in electric vehicles," *IEEE Trans. Power Electron.*, vol. 36, no. 6, pp. 7319–7332, Jun. 2021, doi: 10.1109/TPEL.2020.3041653.
- [8] Y. Shen, J. Xie, T. He, L. Yao, and Y. Xiao, "CEEMD-fuzzy control energy management of hybrid energy storage systems in electric vehicles," *IEEE Trans. Energy Convers.*, early access, Aug. 21, 2024, doi: 10.1109/TEC.2023.3306804.
- [9] Y. Takahashi, "Development of a personal mobility vehicle for short-range transportation support," in *Proc. IEEE Int. Syst.*, vol. 8, Jun. 2016, pp. 295–297, doi: 10.1109/ISMS.2016.37.
- [10] S. Yun, W. Lee, J. Park, and K.-W. Gwak, "Development of a virtual environment co-simulation platform for evaluating dynamic characteristics of self-balancing personal mobility," *IEEE Trans. Veh. Technol.*, vol. 70, no. 4, pp. 2969–2978, Apr. 2021, doi: 10.1109/TVT.2021.3061733.
- [11] S. Kim and F.-S. Kang, "Multifunctional onboard battery charger for plug-in electric vehicles," *IEEE Trans. Ind. Electron.*, vol. 62, no. 6, pp. 3460–3472, Jun. 2015, doi: 10.1109/TIE.2014.2376878.
- [12] T. Q. Pham, C. Nakagawa, A. Shintani, and T. Ito, "Evaluation of the effects of a personal mobility vehicle on multiple pedestrians using personal space," *IEEE Trans. Intell. Transp. Syst.*, vol. 16, no. 4, pp. 2028–2037, Aug. 2015, doi: 10.1109/TITS.2014.2388219.
- [13] Y. Won Chung, M. Young Chung, and D. Keun Sung, "Effect of personal mobility management in mobile communication networks," *IEEE Trans. Veh. Technol.*, vol. 52, no. 5, pp. 1254–1269, Sep. 2003, doi: 10.1109/TVT.2003.816639.
- [14] A. Kuperman, U. Levy, J. Goren, A. Zafransky, and A. Savernin, "Battery charger for electric vehicle traction battery switch station," *IEEE Trans. Ind. Electron.*, vol. 60, no. 12, pp. 5391–5399, Dec. 2013, doi: 10.1109/TIE.2012.2233695.
- [15] J. Min and M. Ordenez, "Bidirectional resonant CLLC charger for wide battery voltage range: Asymmetric parameters methodology," *IEEE Trans. Power Electron.*, vol. 36, no. 6, pp. 6662–6673, Jun. 2021, doi: 10.1109/TPEL.2020.3033982.
- [16] H. Karneddi and D. Ronanki, "Universal bridgeless nonisolated battery charger with wide-output voltage range," *IEEE Trans. Power Electron.*, vol. 38, no. 3, pp. 2816–2820, Mar. 2023, doi: 10.1109/TPEL.2022.3217943.
- [17] S.-K. Lim, H.-S. Lee, H.-R. Cha, and S.-J. Park, "Multi-level DC/DC converter for E-mobility charging stations," *IEEE Access*, vol. 8, pp. 48774–48783, 2020, doi: 10.1109/ACCESS.2020.2977663.
- [18] F. Musavi, M. Craciun, D. S. Gautam, and W. Eberle, "Control strategies for wide output voltage range LLC resonant DC–DC converters in battery chargers," *IEEE Trans. Veh. Technol.*, vol. 63, no. 3, pp. 1117–1125, Mar. 2014, doi: 10.1109/TVT.2013.2283158.
- [19] Y. Bak, "Hardware-simulator development and implementation of battery charger for personal mobility devices," *J. Power Electron.*, vol. 23, pp. 211–218, Feb. 2023, doi: 10.1007/s43236-022-00580-1.
- [20] M.-G. Jeong, S.-H. Kim, and C. Yoo, "Switching battery charger integrated circuit for mobile devices in a 130-nm BCD MOS process," *IEEE Trans. Power Electron.*, vol. 31, no. 11, pp. 7943–7952, Nov. 2016, doi: 10.1109/TPEL.2016.2514518.

- [21] N. Shafiei, M. Ordonez, M. Craciun, C. Botting, and M. Edington, "Burst mode elimination in high-power LLC resonant battery charger for electric vehicles," *IEEE Trans. Power Electron.*, vol. 31, no. 2, pp. 1173–1188, Feb. 2016, doi: [10.1109/TPEL.2015.2420573](https://doi.org/10.1109/TPEL.2015.2420573).
- [22] R. Metidji, B. Metidji, and B. Mendil, "Design and implementation of a unity power factor fuzzy battery charger using an ultrasparse matrix rectifier," *IEEE Trans. Power Electron.*, vol. 28, no. 5, pp. 2269–2276, May 2013, doi: [10.1109/TPEL.2012.2211107](https://doi.org/10.1109/TPEL.2012.2211107).
- [23] B.-Y. Chen and Y.-S. Lai, "New digital-controlled technique for battery charger with constant current and voltage control without current feedback," *IEEE Trans. Ind. Electron.*, vol. 59, no. 3, pp. 1545–1553, Mar. 2012, doi: [10.1109/TIE.2011.2167115](https://doi.org/10.1109/TIE.2011.2167115).
- [24] Y.-H. Jung, J.-H. Jung, H.-E. Jeong, J.-H. Jung, J.-S. An, H.-A. Ahn, S.-K. Hong, and O.-K. Kwon, "A fast and highly accurate battery charger with accurate built-in resistance detection," *IEEE Trans. Power Electron.*, vol. 33, no. 12, pp. 10051–10054, Dec. 2018, doi: [10.1109/TPEL.2018.2830747](https://doi.org/10.1109/TPEL.2018.2830747).
- [25] Z. Huang, G. Wang, J. Yu, and X. Qu, "A novel clamp coil assisted IPT battery charger with inherent CC-to-CV transition capability," *IEEE Trans. Power Electron.*, vol. 36, no. 8, pp. 8607–8611, Aug. 2021.
- [26] P.-J. Liu and L.-H. Chien, "A high-efficiency integrated multimode battery charger with an adaptive supply voltage control scheme," *IEEE Trans. Power Electron.*, vol. 33, no. 8, pp. 6869–6876, Aug. 2018, doi: [10.1109/TPEL.2017.2761816](https://doi.org/10.1109/TPEL.2017.2761816).
- [27] L. Zhang, Q. Yin, W. Zhu, L. Lyu, L. Jiang, L. H. Koh, and G. Cai, "Research on the orderly charging and discharging mechanism of electric vehicles considering travel characteristics and carbon quota," *IEEE Trans. Transp. Electrific.*, early access, Jul. 19, 2023, doi: [10.1109/TTE.2023.3296964](https://doi.org/10.1109/TTE.2023.3296964).
- [28] Y. Bak, Y. J. Lee, and K.-B. Lee, "Dynamic characteristic improvement of phase-shift full-bridge center-tapped converters using a model predictive control," *IEEE Trans. Ind. Electron.*, vol. 69, no. 2, pp. 1488–1497, Feb. 2022, doi: [10.1109/TIE.2021.3057038](https://doi.org/10.1109/TIE.2021.3057038).
- [29] E. Fuentes, C. A. Silva, and R. M. Kennel, "MPC implementation of a quasi-time-optimal speed control for a PMSM drive, with inner modulated-FS-MPC torque control," *IEEE Trans. Ind. Electron.*, vol. 63, no. 6, pp. 3897–3905, Jun. 2016, doi: [10.1109/TIE.2016.2519326](https://doi.org/10.1109/TIE.2016.2519326).
- [30] C. Wang, M. Yang, W. Zheng, J. Long, and D. Xu, "Vibration suppression with shaft torque limitation using explicit MPC-PI switching control in elastic drive systems," *IEEE Trans. Ind. Electron.*, vol. 62, no. 11, pp. 6855–6867, Nov. 2015, doi: [10.1109/TIE.2015.2438055](https://doi.org/10.1109/TIE.2015.2438055).



GWANYOUNG MOON (Student Member, IEEE) received the B.S. degree in electrical energy engineering from Keimyung University, Daegu, South Korea, in 2021, where he is currently pursuing the M.S. degree in electronic and electrical engineering. His current research interests include dc/dc converter, electric machine drives, and grid-connected systems.



YEONGSU BAK (Member, IEEE) received the B.S., M.S., and Ph.D. degrees in electrical and computer engineering from Ajou University, Suwon, South Korea, in 2014, 2016, and 2019, respectively. From 2019 to 2020, he was a Research Associate with the Research Institute for Information and Electronics Technology, Ajou University. In 2020, he joined the Department of Electrical Energy Engineering, Keimyung University, Daegu, South Korea. His current research interests include grid-connected systems, electric machine drives, and matrix converters.

• • •